Determination of the Rate and Yield of B-side Quinone Reduction in *Rhodobacter capsulatus* Reaction Centers†

Hooi Ling Kee,‡ Philip D. Laible,§ James A. Bautista,§ Deborah K. Hanson,§ Dewey Holten,‡ and Christine Kirmaier*,‡

Department of Chemistry, Washington University, St. Louis, Missouri 63130 and Biosciences Division, Argonne National Laboratory, Argonne, Illinois 60439

Received February 9, 2006; Revised Manuscript Received March 31, 2006

ABSTRACT: In the native purple bacterial reaction center (RC), light-driven charge separation utilizes only the A-side cofactors, with the symmetry related B-side inactive. The process is initiated by electron transfer from the excited primary donor (P*) to the A-side bacteriopheophytin ($P^* \rightarrow P^+H_A^-$) in ∼3 ps. This is followed by electron transfer to the A-side quinone ($P^+H_A^- \rightarrow P^+Q_A^-$) in ∼200 ps, with an overall quantum yield of ∼100%. Using nanosecond flash photolysis and RCs from the *Rhodobacter capsulatus* F(L181)Y/Y(M208)F/L(M212)H mutant (designated YFH), we have probed the decay pathways of the analogous B-side state $P^+H_B^-$. The rate of the $P^+H_B^- \rightarrow$ ground-state charge-recombination process is found to be $(3.0 \pm 0.8\ \text{ns})^{-1}$, which is much faster than the analogous $(10-20\ \text{ns})^{-1}$ rate of $P^+H_A^- \rightarrow$ ground state. The rate of $P^+H_B^- \rightarrow P^+Q_B^-$ electron transfer is determined to be $(3.9 \pm 0.9\ \text{ns})^{-1}$, which is about a factor of 20 slower than the analogous A-side process $P^+H_A^- \rightarrow P^+Q_A^-$. The yield of $P^+H_B^- \rightarrow P^+Q_B^-$ electron-transfer calculated from these rate constants is 44%. This value, when combined with the known 30% yield of $P^+H_B^-$ from P* in YFH RCs, gives an overall yield of 13% for B-side charge separation $P^* \rightarrow P^+H_B^- \rightarrow P^+Q_B^-$ in this mutant. We determine essentially the same value (15%) by comparing the P-bleaching amplitude at ∼1 ms in YFH and wild-type RCs.

The bacterial photosynthetic reaction center (RC)[1] protein complex contains two quinone molecules that are the means by which the reducing equivalents produced by light-driven charge separation are stored and shuttled out of the RC. These two quinones (Q_A and Q_B) are situated so that they can serve as the terminal electron acceptors on symmetry-related cofactor chains emanating from the dimeric bacteriochlorophyll primary electron donor (P) (*1*−*4*). However, in the native RC, the ultimate electron acceptor Q_B is reduced only via activity of the A-side cofactors, with the B-side being inactive (Figure 1) (*5*−*8*). The lowest excited singlet state of P (P*) transfers an electron in ∼3 ps to the bacteriopheophytin acceptor (H_A) via monomeric bacteriochlorophyll B_A. Subsequent $P^+H_A^- \rightarrow P^+Q_A^-$ conversion takes place with a time constant of ∼200 ps and is followed by $P^+Q_A^- \rightarrow P^+Q_B^-$ electron transfer on the microsecond time scale. A cytochrome reduces P^+ in vivo to re-arm the A-side primary electron transport chain for a second round of charge separation and delivery of a second electron to Q_B. This acceptor dissociates from the RC as the quinol (Q_BH_2), thus performing its role as a two-electron gate. The B-side cofactors B_B and H_B play no known role in the charge separation functions of the RC.

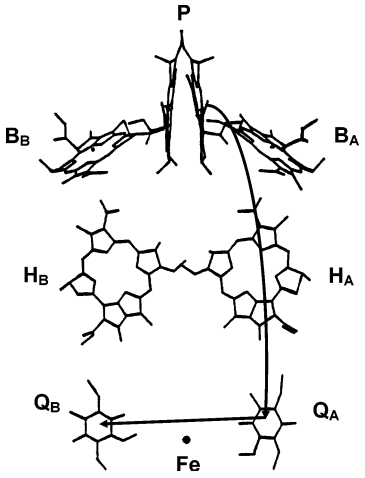

FIGURE 1: Arrangement of the cofactors in the purple bacterial reaction center (*4*). The arrow marks the charge-separation pathway used exclusively in the native RC.

The basic design of two quasi-symmetric branches of potential electron-transfer cofactors is preserved in the pigment−protein complexes of photosystem I (PSI) (*9*, *10*) and photosystem II (PSII) (*11*−*14*). Unlike the bacterial RC and PSII with their unidirectional sequence of primary charge

† This work was supported by Grant MCB-0314588 from the National Science Foundation (C.K. and D.H.) and the U.S. Department of Energy, Office of Biological and Environmental Research, under Contract No. W-31-109-ENG-38 (P.D.L. and D.K.H.).

* To whom correspondence should be addressed. E-mail: kirmaier@wustl.edu; phone: 314-935-6480; fax: 314-935-4481.

‡ Washington University.

§ Argonne National Laboratory.

[1] Abbreviations: RC, reaction center; BChl, bacteriochlorophyll; BPh, bacteriopheophytin; P, primary electron donor, a dimer of BChls; P*, the lowest excited singlet state of P; P^R, the lowest excited triplet state of P; B_A and B_B, monomeric BChls on the A- and B-branches, respectively; H_A and H_B, the A-branch and B-branch BPhs, respectively; Q_A and Q_B, primary and secondary quinone acceptors, respectively; LDAO, *N*-lauryl-*N*,*N*-dimethylamine-*N*-oxide.

10.1021/bi060277x CCC: $33.50
Published on Web 05/19/2006

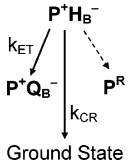

FIGURE 2: Kinetic scheme for decay of $P^+H_B^-$ by electron transfer to yield $P^+Q_B^-$, by charge recombination to form the ground state, and by formation of the triplet excited state of P (P^R). Formation of P^R would involve spin rephasing that converts the singlet form of $P^+H_B^-$ to the triplet form followed by charge recombination. Since we show here that P^R appears to form with a yield ≤ 5% from $P^+H_B^-$ in the YFH RC (see text), this process is ignored in the kinetic analysis.

separation to just one set of cofactors, both electron transport branches may be functional in type I RCs (*15*−*17*). The analogy in the bacterial RC would be a functional P* → $P^+H_B^-$ → $P^+Q_B^-$ electron-transfer pathway. Mutant bacterial RCs in which charge separation from P* to the B-side cofactors has been elicited (*18*−*40*) offer the opportunity to understand the origin of the differences between the rates and the yields of A- and B-side charge separation and may give insight into how PSI has been optimized for bidirectional electron transfer. Ultimately, these principles can be applied to yield a general understanding of protein-mediated electron-transfer reactions and to the design of bioinspired artificial systems for solar-energy conversion. Additionally, B-side electron transfer from H_B^- to Q_B offers possibilities of trapping and studying conformational or protonation states that are not formed or are formed only transiently during the normal course of two-electron and two-proton transfer to Q_B in the native system (*30*, *37*, *38*).

Low yields of electron transfer along the entire B branch (P* → $P^+H_B^-$→ $P^+Q_B^-$) have been reported in a number of mutant RCs (*19*, *30*, *31*, *36*−*39*, *41*). This overall yield is the product of the yields of P* → $P^+H_B^-$ and $P^+H_B^-$ → $P^+Q_B^-$ reactions. From subpicosecond transient absorption studies on the *Rhodobacter* (*R.*) *capsulatus* YFHV mutant (where YFH is as defined below and V denotes mutation of Trp M250 to Val, which results in loss of Q_A), we recently estimated $P^+H_B^-$ → $P^+Q_B^-$ to have a rate constant in the range of $(2-12\ ns)^{-1}$ and a yield in the range of 25−80% (*31*). In the present study, we report more precise determinations of the rate and yield of $P^+H_B^-$ → $P^+Q_B^-$ electron transfer and of the rate and yield of the competing charge-recombination reaction $P^+H_B^-$ → ground state. We have investigated these B-side processes in RCs from the YFH mutant of *R. capsulatus* (*23*, *30*−*32*). This triple mutant combines the swap of the C_2-symmetry-related residues PheL181 near B_B (changed to Tyr), and TyrM208 near B_A (changed to Phe), and replacement of Leu at M212 with His, which causes incorporation of a BChl denoted β in place of H_A. We chose the YFH RC for this study because its 30% yield of $P^+H_B^-$ provides the best current platform for monitoring the decay kinetics of this state and the observation of $P^+Q_B^-$ formation.

Figure 2 shows the competitive processes by which $P^+H_B^-$ can decay. In addition to electron transfer to form $P^+Q_B^-$ (rate constant k_{ET}) and charge separation to give the ground state (rate constant k_{CR}), decay of $P^+H_B^-$ could produce the excited triplet state of P (denoted P^R). Formation of P^R would occur by spin rephasing within the singlet form of the radical-pair state, $^1(P^+H_B^-)$, to the triplet form, $^3(P^+H_B^-)$, a coherent process not characterized by a rate constant, followed by charge recombination. Formation of P^R from B-side charge separation has not yet been reported but is inferred from analogy to the A-side of the wild-type RC where P^R is formed during the ∼10 ns lifetime of $P^+H_A^-$ in ∼10% yield when Q_A is prereduced and in higher yield (∼30%) if the RCs are depleted of Q_A (*42*−*44*). As shown below, we find that the yield of P^R from $P^+H_B^-$ in the YFH mutant is much less than the 10% found in wild-type Q_A-reduced RCs. Thus, the simplified scheme in Figure 2 shows a dashed arrow to P^R reflecting a process that we will ignore in determining the rate constants and yields of $P^+H_B^-$ → $P^+Q_B^-$ electron-transfer and $P^+H_B^-$ → ground-state charge recombination. These rate constants are obtained from comparison of the lifetimes of $P^+H_B^-$ measured in the presence and in the absence of Q_B in the YFH mutant. In this study, we determine both lifetimes from nanosecond flash photolysis experiments that measure the decay of the H_B^- absorption at 640 nm. This type of measurement is technically challenging since lifetimes in the nanosecond range are too long to be determined with confidence with a standard picosecond transient absorption setup using optical delay lines, which typically give data to at most about 5 ns. Measuring the ∼10 ns charge-recombination lifetime of $P^+H_A^-$ when electron transfer to Q_A is blocked is similarly difficult and has been determined principally via delayed fluorescence from P*, with a few reports utilizing the direct transient absorption kinetic method employed here (*42*−*47*). Since we expected the $P^+H_B^-$ lifetime to be much shorter than 10 ns based on our earlier studies (*20*, *23*, *26*, *31*), it was important to utilize a fast-response detection system and a short excitation flash. The small transient signals due to the 30% yield of $P^+H_B^-$ formed from P* add to the difficulty of the measurement. As a check on the results, we also performed independent measurements of the yield of $P^+Q_B^-$ from $P^+H_B^-$ in YFHV RCs relative to that from $P^+Q_A^-$ in wild-type RCs by comparing the initial amplitudes of the P-bleaching decay profiles in millisecond transient absorption experiments.

MATERIALS AND METHODS

RC Samples. All of the RCs studied here have been described previously (*18*, *19*, *23*, *27*, *30*). For the nanosecond lifetime measurements, RCs from wild-type *R. capsulatus* (not polyhistidine-tagged) and the L(M212)H mutant (both His-tagged and untagged versions), and the *R. sphaeroides* L(M214)H mutant (His-tagged) were used as controls. These RCs were isolated using standard LDAO or Deriphat 160-C solubilization and purification protocols with the detergent subsequently exchanged to Triton X-100 by affinity or ion exchange chromatography by washing with 2 L of buffer containing Triton X-100 over a period of several hours. For control measurements of the lifetimes of $P^+H_A^-$ (in wild-type RCs) and $P^+\beta^-$ (in the L(M212)H and L(M214)H mutants), Q_A was reduced immediately before experiments by adding a slight excess of sodium dithionite (from a concentrated, buffered solution) to RCs having an absorption in the near-infrared band of P between 4 and 7 (in a 2 mm path length cuvette; 100 mM potassium phosphate, pH 7.6/0.05% Triton X-100 buffer). Semianaerobic conditions were achieved by repeated cycles of displacing the air in the cuvette above the liquid level of the RCs with nitrogen and gentle inversion of the cuvette. This was done immediately

before the dithionite was added and again after and the cuvette was then stoppered. Repeat measurements on different days utilized fresh RCs with freshly reduced Q_A.

His-tagged RCs from the *R. capsulatus* YFH mutant (bearing the F(L181)Y/Y(M208)F/L(M212)H substitutions) were isolated using the detergent Deriphat 160-C to ensure full occupancy of the Q_B binding pocket and were studied in 10 mM Tris pH 7.8/0.1% Deriphat 160-C buffer (*30*). Again for the nanosecond-lifetime measurements, as well as for studies on the microsecond time scale, these RCs had absorption between 6 and 8 at 865 nm in a 2 mm path length cell. Electron transfer to Q_B was quantitatively inhibited as needed by addition of terbutryn (from a concentrated stock solution in ethanol) to a final concentration corresponding to ~25 RC equivalents. For the measurements that compared the magnitude of 865 nm P-bleaching on the millisecond time scale as an independent determination of the $P^+Q_B^-$ yield in YFH, YFHV and wild-type RCs, the samples had an absorbance at 865-nm of ~0.5 in a 2 mm path length.

Nanosecond Lifetime Measurements. The lifetimes of $P^+H_B^-$, $P^+H_A^-$, and $P^+\beta^-$ (according to sample) were determined on a home-built spectrophotometer with all measurements made at 298 K. Samples were held in a 2 mm path length cuvette with a ~25° angle between the excitation and the probe directions. The 640-nm probe beam was supplied by a laser diode (Thorlabs) passing in order through a shutter (Uniblitz LS2T2), colored and neutral-density filters, the sample, and finally a monochromator abutted to the detector. The intensity of this probe was adjusted with the neutral-density filters before the sample to minimize actinic effects on the RCs while preserving a satisfactory signal-to-noise ratio. An actively/passively mode-locked frequency-doubled Nd:YAG laser (YG 400, Quantel) provided 30-ps, ~3 mJ, excitation flashes at 532 nm. The diameter of the excitation flashes at the sample was large (~5 mm) to ensure complete overlap with the probe and maximal signal amplitude. The laser was operated in "single-shot" mode with sufficient time between successive flashes to allow full recovery of the RCs via dark adaptation. This time ranged from a few seconds to several minutes as appropriate for the RC sample and the experimental conditions. The sequence of events was controlled by a pulse generator (BNC 555), which fired the laser flash lamps and controlled opening and closing of the shutter in the probe beam. The probe shutter was opened for the minimum time necessary for the oscilloscope sweep so as to minimize exposure of the RCs to light.

Signals were acquired by a fast photosensor module (Hamamatsu H6780-20), current-to-voltage amplified (Stanford Research Instruments SR445 (two stages) or Hamamatsu C5594), and recorded on a 1.5 GHz, 20 gigasample/s digital oscilloscope (Tektronics TDS 7154), using 50 Ω input and output impedance at each stage. The overall instrument response time was ~800 ps. Despite extensive optical filtering and care with electronic noise, the signals at early time often contained a contribution from a "flash artifact" that is inevitable in these types of measurements. This contribution was removed by subtraction of the "artifact signal" obtained without probe light and otherwise identical conditions. Note that the transient absorption signal at 640 nm for the H_B anion in state $P^+H_B^-$ is a positive ΔA and is easily distinguished from flash artifacts, fluorescence from impurities, etc., which give signals of the opposite sign. This is one reason we chose to probe the weak anion region absorption decay of $P^+H_B^-$, rather than probing the larger P-bleaching decay at ~865 nm, where the sign of the bleaching signal (negative ΔA) is the same as flash artifacts and fluorescence (from P* or free pigments). Potential actinic effects of the probe light also are reduced significantly at 640 nm compared to 865 nm, where the ground-state absorption is much larger. The amplitudes of the absorbance changes at 640 nm (typically 0.04−0.1) for states $P^+H_B^-$, $P^+H_A^-$, and $P^+\beta^-$ (depending on the RC) were as expected based on transient absorption spectra obtained for the same states in subpicosecond transient absorption studies, taking into account the relative RC concentrations. The decay of the triplet excited state of $RuTPP(pip)_2$, the bispiperidine adduct of ruthenium tetraphenylporphyrin, was used to verify and optimize peak instrument performance at the beginning of every data collection session. The 640-nm triplet−triplet absorption (positive ΔA) of this sample was found to decay with a time constant of 2.3 ± 0.2 ns, in good agreement with the value of 2.0 ± 0.2 ns found previously from picosecond transient absorption studies (*48*). The analogous bispyridine adduct $RuTPP(pyr)_2$ was found to have a lifetime of 16 ± 1 ns, in good agreement with the literature value of 15 ± 2 ns (*48*). As mentioned above, additional control measurements utilized *R. capsulatus* wild-type and L(M212)H mutant RCs and *R. sphaeroides* L(M214)H RCs with Q_A prereduced, for which the $P^+H_A^-$ (in wild-type RCs) and $P^+\beta^-$ (the mutants) lifetimes are previously determined or anticipated to be in the range of ~1 to ~20 ns (*42*−*45*, *49*−*54*).

For all samples, the time profiles from 25 single laser shot data acquisitions were collected and averaged together on the oscilloscope, and then saved as an individual decay trace (a "trial"). To fit "complete" data sets, 25 single-shot "flash-artifact" signals (i.e., no probe light) were similarly averaged on the oscilloscope and saved, and then subtracted from the "trial" experimental data files, and the resulting decay traces were fit to the sum of a Gaussian instrument profile plus a single exponential plus a constant (IgorPro, Wavemetrics). Alternatively, the same lifetimes were obtained by subtracting the flash artifact and deleting the time points encompassing the instrument profile, and fitting the remainder to a single exponential plus a constant (Origin, Microcal), and this method was used for the majority of the analyses. Five to 10 "trial" decay traces were acquired during a single day on a freshly prepared sample depending on the length of time required between flashes for full dark-adaptation. For each RC, measurements were made on three to five freshly prepared samples. The fit results of all of these trials were averaged to give the reported values and error bars for the lifetimes. For measurements to assess evidence for the triplet state P^R on the microsecond time scale, either the same setup described above was employed, or an improved signal-to-noise (but a slower ~50 ns) response was obtained by utilizing a single stage of the SR445 amplifier with a 500 Ω input impedance (used to acquire the data in the insets to Figure 3).

Yield of $P^+Q_B^-$ Determined by the Magnitude of P-Bleaching in the Millisecond Regime. The amplitude of ground-state bleaching of P at 865 nm was measured at ~1 ms following excitation using the experimental setup de-

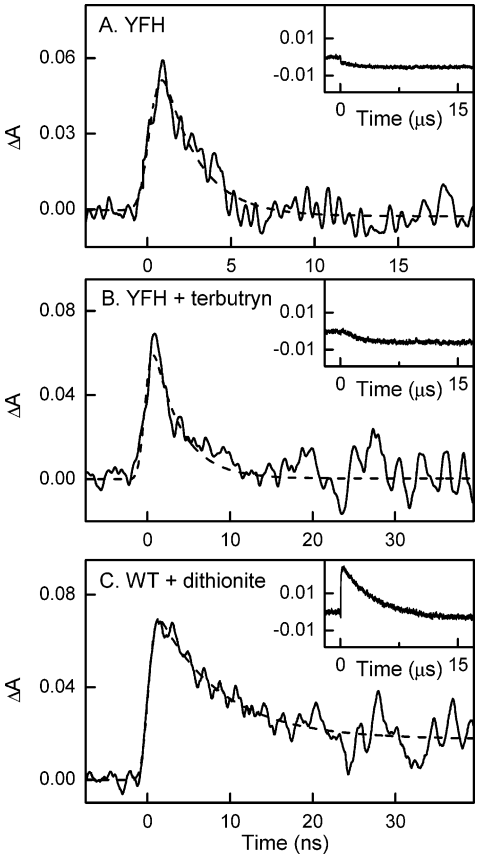

FIGURE 3: Decay kinetics of $P^+H_B^-$ in YFH RCs in Deriphat 160-C at room temperature following 30-ps 532-nm excitation in the absence (A) or presence (B) of terbutryn, a competitive inhibitor of Q_B binding, and of $P^+H_A^-$ in wild-type RCs with added sodium dithionite (C). Each data trace (solid lines) is the average of 25 single laser shot data acquisitions that have had the flash artifact subtracted (see text). The dashed lines are fits to the instrument response plus an exponential plus a constant with fit values of the time constants of 2.1 ns (A), 3.2 ns (B) and 7.7 ns (C). The insets show the kinetic profiles obtained on the microsecond time scale for the same RCs but utilizing a slower-response lower noise detection scheme. See text for more details.

scribed above with a few minor modifications. A 100 W quartz tungsten halogen lamp supplied the 865 nm probe light. Again, a shutter and appropriate filters controlled the intensity and duration of the probe light at the sample to minimize actinic effects. Filters and a monochromator (1/4 m Jarell Ash) after the sample were employed to minimize the stray light that reached the photosensor module detector. The current output of the detector was input directly to a 500 MHz, 1 MΩ input of the digital oscilloscope. Typically, 5−10 single laser shot excitations were acquired and averaged together on any one sample. Firing of the laser was controlled manually (again with sufficient time between successive runs to allow full recovery of the RC to the ground state). Typically, sweeps of 10 ms/division were used to determine the initial amplitudes of the absorbance changes due to the formation of $P^+Q_B^-$ or $P^+Q_A^-$ (or a combination), and longer sweeps (to 40 s/div) were used to assess the decay kinetics.

RESULTS AND DISCUSSION

$P^+H_B^-$ Lifetime Measurements. Kinetic decay profiles were recorded at 640 nm following a 30 ps excitation flash at 532 nm. These measurements probe the absorption in the anion band of H_B (YFH RCs) or β or H_A as appropriate to the state formed in the individual RC as indicated in Table 1. The anion of each of these pigments has a broad absorption band extending from ~600 to ~700 nm, with H_B^- peaking near 640 nm, H_A^- near 665 nm, and β^- near 660 and 680 nm (*23*, *55*). The lifetimes determined are collected in Table 1. Figure 3 (main panels) shows representative decay profiles for YFH and wild-type RCs and fits of the data to the instrument response plus a single-exponential plus a constant. The wild-type and two "beta" mutant RCs listed in Table 1 served as controls for comparison, and we describe them first. In these RCs, the lifetime of the A-side state $P^+H_A^-$ or $P^+\beta^-$ was measured under conditions where Q_A was prereduced by the addition of sodium dithionite. For Q_A-reduced *R. capsulatus* L(M212)H and *R. sphaeroides* L(M214)H RCs, we find $P^+\beta^-$ lifetimes of 4 ± 2 and 1.2 ± 0.4 ns, respectively. The $P^+\beta^-$ lifetime in Q_A-reduced *R. capsulatus* L(M212)H RCs has not been measured previously but was predicted to be roughly 1 ns based on the $P^+\beta^-$ lifetime (210 ps) and $P^+Q_A^-$ yield in RCs in which Q_A is active (*18*, *52*, *56*), and is thought to be <5 ns because no triplet EPR signals arising from P^R are observed following $P^+\beta^-$ decay (Laible, P. D., unpublished observations). Previous picosecond transient absorption studies gave a $P^+\beta^-$ lifetime in prereduced *R. sphaeroides* L(M214)H RCs of 0.9 ns, accompanied by >95% ground-state recovery with little or no P^R formation (*50*, *51*, *53*). For Q_A-reduced wild-type *R. capsulatus* RCs, we find 8 ± 1 ns for the $P^+H_A^-$ lifetime. This is close to the range of values (typically 10−13 ns) determined previously for *R. sphaeroides* RCs with Q_A prereduced, most often from delayed fluorescence measurements (*43*, *45*, *54*). In some cases, somewhat longer lifetimes have been obtained for wild-type *R. sphaeroides* RCs depleted of Q_A by chemical treatment (*42*, *44*, *49*). Previous studies of prereduced wild-type *R. sphaeroides* RCs indicate that the ~10 ns $P^+H_A^-$ lifetime reflects a combination of ground-state recovery and formation of P^R, as described above (*42*−*44*). P^R has a transient absorbance difference spectrum (*43*) similar to that of the singlet excited state of P, P* (see, e.g., refs *23* and *31*) and the excited states of isolated bacteriochlorin pigments (*43*, *57*, *58*). In particular, it has a small featureless positive absorption throughout the 500−800 nm visible region. Hence, the $P^+H_A^-$ decay trace at 640 nm in Figure 3C has a small positive asymptotic value we assign to formation of P^R. We measure a 4.5 μs time constant for decay of this transient absorption (Figure 3C inset), which compares well with the reported P^R lifetime of ~7 μs in *R. sphaeroides* Q-reduced RCs (*43*, *59*). Although the lack of precise values for the relative extinction coefficients of $P^+H_A^-$ and P^R at 640 nm prevents us from

Table 1: Lifetime Summary

sample	strain	additions	state	lifetime (ns)
YFH[a]	*R. capsulatus*	none	$P^+H_B^-$	1.7 ± 0.5
YFH[a]	*R. capsulatus*	terbutryn	$P^+H_B^-$	3.0 ± 0.8
L(M212)H[b,c]	*R. capsulatus*	$Na_2S_2O_4$	$P^+\beta^-$	4 ± 2
L(M214)H[b,c]	*R. sphaeroides*	$Na_2S_2O_4$	$P^+\beta^-$	1.2 ± 0.4
WT[b]	*R. capsulatus*	$Na_2S_2O_4$	$P^+H_A^-$	8 ± 1

[a] Samples in Deriphat 160-C at room temperature. [b] Samples in Triton X-100. [c] M214 in *R. sphaeroides* is the same as M212 in *R. capsulatus*, the so-called "beta" mutants.

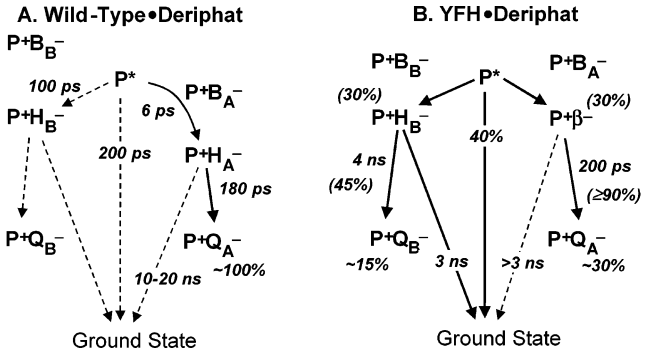

FIGURE 4: Summary of the primary photochemistry in (A) wild-type and (B) YFH RCs in Deriphat 160-C at room temperature determined from previous studies and those presented here. The rate constants and yields of P* decay are somewhat different for each RC in LDAO (*23*, *32*).

determining the yield of P^R from these data, they are consistent with the expected low (~10%) yield of P^R. The literature values for the $P^+H_A^-$ lifetime and P^R yield (supported by our results) indicate that the rate constant for $P^+H_A^-$ charge recombination to the ground state in the native RC is on the order of $(10-20\ ns)^{-1}$, as is indicated in Figure 4A.

For the YFH mutant in Deriphat, the $P^+H_B^-$ lifetime is 1.7 ± 0.5 ns with Q_B present (Figure 3A) and 3.0 ± 0.8 ns when electron transfer to Q_B is blocked by the addition of terbutryn, a competitive inhibitor of Q_B binding (Figure 3B). Before analyzing these results further, we discuss the rationale behind using YFH RCs and the conditions employed. As noted in the introduction, the 30% $P^+H_B^-$ yield for the YFH RC is one of the highest obtained to date. $P^+H_B^-$ is the sole state being probed on the nanosecond time scale in these measurements, as follows from consideration of the photochemistry. Following excitation of P in YFH RCs that have been isolated with the detergent Deriphat 160-C, P* decays in a trifurcated manner: 40% undergoes internal conversion to the ground state, and $P^+H_B^-$ (on the B-side) and $P^+\beta^-$ (on the A-side) are both formed in 30% yield (Figure 4B). The A-side state $P^+\beta^-$ decays in ~180 ps via electron transfer to Q_A in ≥90% yield, with ≤10% charge recombination to the ground state. Thus, contribution of $P^+\beta^-$ to the transient absorption signal occurs within the response time of the instrument and is insignificant on the nanosecond time scale of the $P^+H_B^-$ lifetime measurement. Similarly, the $P^+Q_A^-$ state formed on the A-side decays either on the microsecond time scale (by electron transfer to Q_B if present) or on the millisecond time scale (by charge recombination to the ground state if Q_B is absent), so the transient absorption signal at 640 nm due to this state would not contribute to the kinetics on the nanosecond time scale. Thus, $P^+H_B^-$ is the only state in YFH RCs that reports in the data presented in the main panels of Figure 3A,B. It is worth noting that this would not hold for YFH RCs in which Q_A was prereduced or absent (e.g., the YFHV mutant, which lacks Q_A). Excitation of such a sample would yield a roughly equal mixture of $P^+H_B^-$ on the B-side, and, on the A-side, $P^+\beta^-$ having a lifetime of 1−4 ns based on the data in Table 1. The presence of this mixture of charge-separated states with very similar lifetimes would make it essentially impossible to determine the $P^+H_B^-$ lifetime with any degree of accuracy. The problem is avoided by having functional Q_A.

Unlike the data for the wild-type RC in Figure 3C, the YFH mutant both with and without added terbutryn gives kinetic traces that decay roughly to $\Delta A = 0$ at ~25 ns (Figure 3A,B). The insets to Figure 3A,B also show that compared to wild type (Figure 3C), there is only a very small signal that may decay on the microsecond time scale. (Any small residual negative ΔA is due to the $P^+Q_A^-$ formed within the instrument response by A-side charge separation.) By this measure and in comparison to wild type, P^R is formed in the YFH mutant with a yield of ≤5% in the presence of terbutryn and even less in its absence. Because the yield is so low (and since the formation of P^R is not strictly characterized by a rate constant), we will ignore it in calculating the rate constants of the $P^+H_B^-$ decay pathways from the lifetime data. In this regard, the values for k_{CR} and k_{ET} that we obtain would be within the reported error bars upon inclusion of even a 10% yield of P^R. Thus, using the kinetic model in Figure 2, we equate the 3.0 ± 0.8 ns $P^+H_B^-$ lifetime obtained for the YFH RC in the presence of terbutryn with the rate constant for $P^+H_B^-$ charge recombination to the ground state. In other words, $k_{CR} = (3.0 \pm 0.8\ ns)^{-1}$. The 1.7 ± 0.5 ns $P^+H_B^-$ lifetime obtained when Q_B is present is given by $(k_{ET} + k_{CR})^{-1}$ with the yield of electron transfer $\phi_{ET} = k_{ET}/(k_{ET} + k_{CR})$ and the yield of charge recombination $\phi_{CR} = k_{CR}/(k_{CR} + k_{ET})$. Hence, the values of our measured lifetimes give $k_{ET} = (1.7 \pm 0.5\ ns)^{-1} - (3.0 \pm 0.8\ ns)^{-1} = (3.9 \pm 0.9\ ns)^{-1}$, $\phi_{ET} = 44 \pm 16\%$, and $\phi_{CR} = 56 \pm 21\%$. The 44% yield of the $P^+H_B^- \rightarrow P^+Q_B^-$ electron-transfer step combines with the $30 \pm 5\%$ yield of $P^* \rightarrow P^+H_B^-$ that we have determined previously (*23*, *32*), to predict a $13 \pm 5\%$ yield of $P^+Q_B^-$ from B-side $P^* \rightarrow P^+H_B^- \rightarrow P^+Q_B^-$ conversion in the YFH RC. These results are consistent with, and refine significantly, the relatively wide ranges of values that we estimated previously from subpicosecond transient absorption measurements on Deriphat-isolated YFH RCs: $k_{CR} = (1.5-3.0\ ns)^{-1}$, $k_{ET} = (2-12\ ns)^{-1}$, $\phi_{ET} = 25-80\%$, and a total yield of $P^* \rightarrow P^+H_B^- \rightarrow P^+Q_B^-$ charge separation of 10−25% (*31*). Figure 4 summarizes some of the salient features of the overall photochemistry of the YFH mutant and compares them with those for the wild-type RC.

$P^+Q_B^-$ Yield Determination from the P-Bleaching Amplitude at 865 nm. As a check on the above results, we determined the yield of $P^+Q_B^-$ in YFH and YFHV RCs by simple and direct comparison of the magnitude of long-lived (millisecond time scale) P-bleaching at 865 nm relative to that obtained for wild-type RCs. The various samples were carefully matched to have the same ground-state absorption at the 865 nm probe wavelength (see Materials and Methods), with small differences in absorption (10% or less) taken into account in analysis of the results. All the RCs used were isolated with Deriphat 160-C to ensure full occupancy of the Q_B site. The goal of these experiments was to measure independently the overall yield of $P^+Q_B^-$ via the B-side and thereby verify the 13% yield determined from the lifetime measurements presented above. This measurement also affords a check on the ratio of the rate constants k_{ET} and k_{CR}, and on the 30% yield of $P^+H_B^-$ from P* taken from our previous measurements. Figure 5 shows representative data. As before, the data were collected following a single 30-ps excitation flash at 532 nm. The use of a short 30-ps excitation flash eliminates "recycling" of the photochemistry that would occur (for some RCs and conditions) due to decay

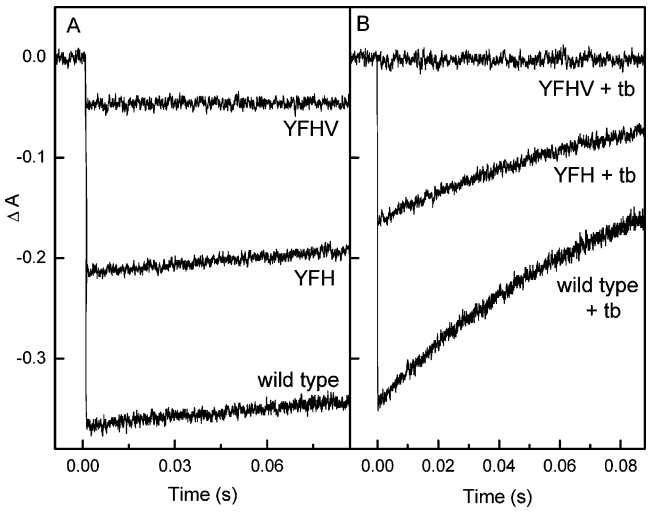

FIGURE 5: Initial amplitudes of the P-bleaching decay profiles (A) and $P^+Q_A^-$ decay profiles in the presence of ~25 equivalents of terbutryn (tb) (B) at 850 nm for RCs in Deriphat 160-C at room temperature following excitation with a 30 ps flash at 532 nm. For YFHV RCs with added terbutryn, there is no signal because both quinones are absent; terbutryn occupies the Q_B binding site and Q_A is not bound due to the W(M250)V mutation.

Table 2: Relative Yields of P^+Q^- States

sample[a]	865-nm P bleaching observed at ~1 ms[b]	state formed	% yield relative to wild type
wild type	−0.365	$P^+Q_B^-$	100%
YFH	−0.210	$P^+Q_B^-$	57 ± 7
YFH + tb[c]	−0.146	$P^+Q_A^-$	40 ± 8
YFHV	−0.055	$P^+Q_B^-$	15 ± 3
YFHV + tb[c]	0	n.a.	0 ± 2

[a] Samples in Deriphat 160-C at room temperature. [b] Bleaching magnitude measured following excitation with a 30 ps flash at 532 nm. [c] tb, terbutryn.

of the charge-separated intermediates ($P^+H_B^-$, $P^+H_A^-$, $P^+\beta^-$) to the ground state on the nanosecond time scale, followed by re-excitation within the duration of a longer flash. The use of 30 ps flashes reduces but does not completely eliminate potential recycling that could occur for a fraction of P* that decays to the ground state in competition with electron transfer to the B or A branches (e.g., the P* lifetime in YFH RCs is ~15 ps). If recycling were significant, we would expect the apparent yield of $P^+Q_B^-$ from these measurements to be skewed to higher values than that obtained from the time-resolved studies.

The yields of charge separation in column 4 of Table 2 are obtained by comparing the magnitude of 865-nm bleaching of the mutant RC to that of wild-type RC at ~1 ms (values in column 2 of Table 2). We will consider each RC in turn and compare the current results with the results obtained from previous work and those given in the previous section. The YFHV RC contains the W(M250)V mutation (tryptophan M250 changed to valine) that prevents binding of Q_A (*19*, *30*). In these RCs, a long-lived charge-separated product can be only $P^+Q_B^-$ as formed by B-side electron transfer. As is seen in Figure 5A, the magnitude of P bleaching in YFHV RCs is ~15% that of wild type, directly determining a yield of $P^+Q_B^-$ in YFHV RCs of 15 ± 3%. This is in excellent agreement with the 13 ± 5% yield determined above from analysis of the $P^+H_B^-$ decay kinetics and an initial ~30% yield of $P^+H_B^-$ in the YFH or YFHV RC (determined in ref *32*). When terbutryn is added to YFHV RCs (Figure 5B), there is no long-lived bleaching of P, as expected. This follows from the discussion given above for YFHV RCs, wherein both $P^+H_B^-$ and $P^+\beta^-$ formed from P* decay on the nanosecond time scale (lifetimes of 1.7 and 4 ns, respectively) and leave no bleaching of P on the millisecond time scale of the data shown in Figure 5.

The data obtained with the Deriphat-isolated YFH mutant RCs also fit consistently with our analysis. Again, we refer to our earlier work showing the products of P* in Deriphat-isolated YFH RCs to be a 40 ± 5% yield of internal conversion to the ground state, and 30 ± 5% yields of both $P^+H_B^-$ and $P^+\beta^-$ (*32*). Thus, in YFH RCs, the magnitude of P-bleaching recorded in Figure 5A should be the sum of the 30 ± 5% yield of electron transfer to Q_B that comes via the A-side, plus the amount that comes via the B-side (15 ± 3%). From data such as those shown in Figure 5, we determine a total yield of 57 ± 7% (Table 2), which is slightly higher than the 45 ± 8% expected (but within experimental error). Similarly, in the YFH RC with terbutryn added (Figure 5), the bleaching magnitude should reflect solely the yield of the A-side electron-transfer product $P^+Q_A^-$. This is found to be 40 ± 8% and again is only about 10% higher than the product of the 30% yield of $P^+\beta^-$ and ≥90% yield of $P^+\beta^- \rightarrow P^+Q_A^-$ taken from our previous work. Overall, these results are consistent within the experimental error of the various measurements.

A related interesting point, again pertaining to charge separation to the A-side in YFH RCs, is our previous finding of slightly different yields of the decay pathways of P* when the protein is solubilized in LDAO as compared to Deriphat (*23*, *31*, *32*). For LDAO-purified YFH RCs, there is a much smaller loss via initial P* → ground state (10% or less), with again a 30% yield of $P^+H_B^-$ formation and the remaining 60−70% giving charge separation to the A-side ($P^+\beta^-$). As a check on this difference in the primary stage of YFH photochemistry, we also examined the initial amplitudes of the charge-separated states at ~1 ms for LDAO-isolated YFH RCs and found a magnitude of P-bleaching that is about 60% that of the wild type (data not shown). This bleaching amplitude reflects $P^+Q_A^-$ formation from $P^+\beta^-$ with no additional contribution of $P^+Q_B^-$ formed via the B-side, since the RCs lose Q_B upon solubilization with LDAO and we made no attempt to reconstitute it. This experiment verifies the difference in branching ratios for the P* decay pathways that we reported previously for the YFH mutant depending on the detergent used for initial RC purification.

Factors Influencing the Decay Characteristics of $P^+H_B^-$. Previously, we have discussed a number of likely architectural and energy-related contributions to the electronic and Franck−Condon factors for the $P^+H_B^- \rightarrow P^+Q_B^-$ electron transfer and $P^+H_B^- \rightarrow$ ground-state charge-recombination processes that may differ from those for the analogous A-side reactions (*23*, *31*). We will not reiterate these or present related possibilities here. However, it is useful to consider that the B-side in the YFH mutant is essentially identical to that of the wild-type B-side in terms of the amino acid environments of H_B and Q_B. In principle, the rate of the $P^+H_B^- \rightarrow$ ground-state reaction and perhaps the rate of the $P^+H_B^- \rightarrow P^+Q_B^-$ reaction could be influenced by the presence of the "Y" mutation F(L181)Y near B_B, which

should lower the free energy of $P^+B_B^-$. This shift would bring this state closer to $P^+H_B^-$ than it is in the wild-type RC, increasing thermal or quantum mechanical mixing between these states.

Let us first consider the potential effect of the increased mixing between $P^+B_B^-$ and $P^+H_B^-$ in the YFH mutant RC compared to the situation on the wild-type B-side. We can glean insights from our prior studies on A-side mutants in which the free energy gap between the A-side charge-separated states ($P^+B_A^-$ and $P^+H_A^-$ or $P^+\beta^-$) is decreased and mixing between them increased (*50*−*53*, *56*, *60*). The result is that the rate of electron transfer to Q_A is altered (reduced) by less than a factor of 2. Extrapolating this observation to the B-side would imply that, other things being equal, $P^+H_B^-\rightarrow P^+Q_B^-$ electron transfer in the YFH RC would be within a factor of 2 of the $\sim(200\ \text{ps})^{-1}$ rate constant in the wild-type RC. Since we found here a much smaller rate constant of $(3.9\ \text{ns})^{-1}$, there must be other significant differences in structural/energetic factors for this process compared to the analogous A-side reaction $P^+H_A^-\rightarrow P^+Q_A^-$ in the native RC. One potential contribution is the presence of a tryptophan residue between H_A and Q_A (Trp M250) that is absent in the symmetry-related position between H_B and Q_B (Phe L216). Initial studies on RCs incorporating a Trp at L216 indicate that it *reduces* the binding affinity of Q_B (*30*).

Increased mixing between $P^+B_B^-$ and $P^+H_B^-$ in the YFH mutant RC compared to the wild-type RC [due to the F(L181)Y mutation] could have a more significant effect on the rate constant for $P^+H_B^-\rightarrow$ ground-state charge recombination. Again, this view is based on the observations for mutants in which H_A is replaced by a bacteriochlorophyll β (*50*−*53*, *56*) and related RCs having altered A-side free energy gaps (*61*−*64*). For example, the increased free energy of $P^+\beta^-$ (compared to $P^+H_A^-$) and consequent increased thermal/quantum mixing with $P^+B_A^-$ has been proposed to underlie the increased rate of charge recombination, from $(10-20\ \text{ns})^{-1}$ for $P^+H_A^-$ in the wild-type RC to $\sim(1-3\ \text{ns})^{-1}$ for $P^+\beta^-$ in the β-containing mutants [*R. sphaeroides* L(M214)H and *R. capsulatus* L(M212)H]. The $P^+H_B^-$ charge recombination rate in the *R. capsulatus* YFH mutant RC is comparable to that for $P^+\beta^-$ in the L(M212)H mutant (Table 1). This finding suggests that decreased free energy gap between it and $P^+B_B^-$ in the YFH RC (due to the stabilizing effect of the F(L181)Y mutation on $P^+B_B^-$) may enhance $P^+H_B^-$ charge recombination compared to the situation on the B-side in the wild-type RC. Future studies using the techniques employed here will test this hypothesis in mutant RCs in which the energy gap between $P^+H_B^-$ and $P^+B_B^-$ is modulated.

CONCLUSIONS

We have determined that the rate of $P^+H_B^-\rightarrow P^+Q_B^-$ electron transfer is $(3.9 \pm 0.9\ \text{ns})^{-1}$, which is about 20-fold slower than the $\sim(200\ \text{ps})^{-1}$ rate of $P^+H_A^-\rightarrow P^+Q_A^-$ electron transfer. We find that the rate of the $P^+H_B^-\rightarrow$ ground-state charge-recombination reaction is $(3.0 \pm 0.8\ \text{ns})^{-1}$ in the YFH RC, which is much faster than the $(10-20\ \text{ns})^{-1}$ rate for the $P^+H_A^-\rightarrow$ ground-state charge-recombination reaction in the native RC. Whereas the competitive rate constants on the A-side of the wild-type RC effectively suppress the $P^+H_A^-\rightarrow$ ground-state process and support 100% yield of fast $P^+H_A^-\rightarrow P^+Q_A^-$ electron transfer, B-side $P^+H_B^-\rightarrow P^+Q_B^-$ electron transfer occurs with a yield of ∼45% in the YFH mutant RC. It is not surprising that $P^+H_B^-\rightarrow P^+Q_B^-$ electron transfer does not occur with ∼100% yield since this is not a functional process of the native RC requisite for photoautotrophic growth of the organism. The function of Q_B is to receive two electrons from reduced Q_A in successive turnovers of the RC photochemistry and dissociate from the RC as the quinol (Q_BH_2). The work presented here and previously demonstrates that not only is $P^*\rightarrow P^+H_B^-$ charge separation suppressed in the native RC, but any $P^+H_B^-$ that might be produced is not optimized for subsequent charge separation to form $P^+Q_B^-$.

REFERENCES

1. Deisenhofer, J., Epp, O., Miki, K., Huber, R., and Michel, H. (1985) Structure of the protein subunits in the photosynthetic reaction center from *Rhodopseudomonas viridis* at 3 Å resolution, *Nature 318*, 618−624.
2. Allen, J. P., Feher, G., Yeates, T. O., Komiya, H., and Rees, D. C. (1987) Structure of the reaction center from *Rhodobacter Sphaeroides* R-26: The cofactors, *Proc. Natl. Acad. Sci. U.S.A. 84*, 5730−5734.
3. Chang, C.-H., El-Kabbani, O., Tiede, D. M., Norris, J. R., and Schiffer, M. (1991) The structure of the membrane-bound photosynthetic reaction center from *Rhodobacter sphaeroides* R-26, *Proc. Natl. Acad. Sci. U.S.A. 30*, 5352−5360.
4. Ermler, U., Fritsch, G., Buchanan, S. K., and Michel, H. (1994) Structure of the photosynthetic reaction centre from *Rhodobacter sphaeroides* at 2.65 Å resolution: Cofactors and protein−cofactor interactions, *Structure 2*, 925−936.
5. Woodbury, N. W., and Allen, J. P. (1995) The Pathway, kinetics, and thermodynamics of electron transfer in wild-type and mutant reaction centers of purple nonsulfur bacteria, in *Anoxygenic Bacteria* (Blankenship, R. E., Madigan, M. T., and Bauer, C. E., Eds.) pp 527−557, Kluwer Academic Publishers, Dordrecht.
6. Parson, W. W. (1996) Photosynthetic bacterial reaction centres, in *Protein Electron Transfer* (Bendall, S. D., Ed.) pp 125−160, BIOS Scientific Publishers, Oxford.
7. Hoff, A. J., and Deisenhofer, J. (1997) Photophysics of photosynthesis. Structure and spectroscopy of reaction centers of purple bacteria, *Phys. Rep. 287*, 1−247.
8. Van Brederode, M. E., and Jones, M. R. (2000) Reaction centres of purple bacteria, *Subcell. Biochem. 35*, 621−676.
9. Jordan, P., Fromme, P., Witt, H. T., Klukas, O., Saenger, W., and Krauss, N. (2001) Three-dimensional structure of cyanobacterial photosystem I at 2.5 angstrom resolution, *Nature 411*, 909−917.
10. Ben-Shem, A., Frolow, F., and Nelson, N. (2003) Crystal structure of plant photosystem I, *Nature 426*, 630−635.
11. Zouni, A., Witt, H. T., Kern, J., Fromme, P., Krauss, N., Saenger, W., and Orth, P. (2001) Crystal structure of photosystem II from *Synechococcus elongatus* at 3.8 angstrom resolution, *Nature 409*, 739−743.
12. Kamiya, N., and Shen, J. R. (2003) Crystal structure of oxygen-evolving photosystem II from *Thermosynechococcus vulcanus* at 3.7-angstrom resolution, *Proc. Natl. Acad. Sci. U.S.A. 100*, 98−103.
13. Ferreira, K. N., Iverson, T. M., Maghlaoui, K., Barber, J., and Iwata, S. (2004) Architecture of the photosynthetic oxygen-evolving center, *Science 303*, 1831−1838.
14. Barber, J., Ferreira, K., Maghlaoui, K., and Iwata, S. (2004) Structural model of the oxygen-evolving centre of photosystem II with mechanistic implications, *Phys. Chem. Chem. Phys. 6*, 4737−4742.
15. Tommos, C., and Babcock, G. T. (2000) Proton and hydrogen currents in photosynthetic water oxidation, *Biochim. Biophys. Acta 1458*, 199−219.
16. Grotjohann, I., Jolley, C., and Fromme, P. (2004) Evolution of photosynthesis and oxygen evolution: Implications from the structural comparison of Photosystems I and II, *Phys. Chem. Chem. Phys. 6*, 4743−4753.
17. Raval, M. K., Biswal, B., and Biswal, U. C. (2005) The mystery of oxygen evolution: Analysis of structure and function of

Photosystem II, the water-plastoquinone oxido-reductase, *Photosynth. Res. 85*, 267−293.
18. Heller, B. A., Holten, D., and Kirmaier, C. (1995) Control of electron transfer to the L-side versus the M-side of the photosynthetic reaction center, *Science 269*, 940−945.
19. Laible, P. D., Kirmaier, C., Holten, D., Tiede, D. M., Schiffer, M., and Hanson, D. K. (1998) Formation of $P^+Q_B^-$ via B-branch electron transfer in mutant reaction centers, in *Photosynthesis: Mechanisms and Effects* (Garab, G., Ed.) pp 849−852, Kluwer Academic Publishers, Dordrecht.
20. Kirmaier, C., Weems, D., and Holten, D. (1999) M-side electron transfer in reaction center mutants with a lysine near the nonphotoactive B bacteriochlorophyll, *Biochemistry 38*, 11516−11530.
21. Katilius, E., Turanchik, T., Lin, S., Taguchi, A. K. W., and Woodbury, N. W. (1999) B-side electron transfer in a *Rhodobacter sphaeroides* reaction center mutant in which the B-Side monomer bacteriochlorophyll is replaced with bacteriopheophytin, *J. Phys. Chem. B 103*, 7386-7389.
22. Roberts, J. A., Holten, D., and Kirmaier, C. (2001) Primary events in photosynthetic reaction centers with multiple mutations near the photoactive electron carriers, *J. Phys. Chem. B 105*, 5575−5584.
23. Kirmaier, C., He, C., and Holten, D. (2001) Manipulating the direction of electron transfer in the bacterial reaction center by swapping Phe for Tyr Near $BChl_M$ (L181) and Tyr for Phe Near $BChl_L$ (M208), *Biochemistry 40*, 12132−12139.
24. Katilius, E., Katiliene, Z., Lin, S., Taguchi, A. K. W., and Woodbury, N. W. (2002) B side electron transfer in a *Rhodobacter sphaeroides* reaction center mutant in which the B side monomer bacteriochlorophyll is replaced with bacteriopheophytin: low-temperature study and energetics of charge-separated states, *J. Phys. Chem. B 106*, 1471−1475.
25. Katilius, E., Katiliene, Z., Lin, S., Taguchi, A. K. W., and Woodbury, N. W. (2002) B-side electron transfer in the HE(M182) reaction center mutant from *Rhodobacter sphaeroides*, *J. Phys. Chem. B 106*, 12344−12350.
26. Kirmaier, C., Cua, A., He, C., Holten, D., and Bocian, D. F. (2002) Probing M-branch electron transfer and cofactor environment in the bacterial photosynthetic reaction center by the addition of a hydrogen bond to the M-side bacteriopheophytin, *J. Phys. Chem. B 106*, 495−503.
27. Kirmaier, C., Laible, P. D., Czarnecki, K., Hata, A. N., Hanson, D. K., Bocian, D. F., and Holten, D. (2002) Comparison of M-side electron transfer in *Rb. sphaeroides* and *Rb. capsulatus* reaction centers, *J. Phys. Chem. B 106*, 1799−1808.
28. de Boer, A. L., Neerken, S., de Wijn, R., Permentier, H. P., Gast, P., Vijgenboom, E., and Hoff, A. J. (2002) High yield of B-branch electron transfer in a quadruple reaction center mutant of the photosynthetic bacterium *Rhodobacter sphaeroides*, *Biochemistry 41*, 3081−3088.
29. de Boer, A. L., Neerken, S., de Wijn, R., Permentier, H. P., Gast, P., Vijgenboom, E., and Hoff, A. J. (2002) B-branch electron transfer in reaction centers of *Rhodobacter sphaeroides* assessed with site-directed mutagenesis, *Photosynth. Res. 71*, 221−239.
30. Laible, P. D., Kirmaier, C., Udawatte, C. S. M., Hofman, S. J., Holten, D., and Hanson, D. K. (2003) Quinone reduction via secondary B-branch electron transfer in mutant bacterial reaction centers, *Biochemistry 42*, 1718−1730.
31. Kirmaier, C., Laible, P. D., Hanson, D. K., and Holten, D. (2003) B-side charge separation in bacterial photosynthetic reaction centers: nanosecond-timescale electron transfer from H_B^- to Q_B, *Biochemistry 42*, 2016−2024.
32. Kirmaier, C., Laible, P. D., Hinden, E., Hanson, D. K., and Holten, D. (2003) Detergent effects on primary charge separation in wild-type and mutant *Rhodobacter capsulatus* reaction centers, *Chem. Phys. 294*, 305−318.
33. Wakeham, M. C., Goodwin, M. G., McKibbin, C., and Jones, M. R. (2003) Photoaccumulation of the $P^+Q_B^-$ radical pair state in purple bacterial reaction centres that lack the Q_A uniquinone, *FEBS Lett. 540*, 234−240.
34. Katilius, E., Babendure, J. L., Lin, S., and Woodbury, N. W. (2004) Electron-transfer dynamics in *Rhodobacter sphaeroides* reaction center mutants with a modified ligand for the monomer bacteriochlorophyll on the active side, *Photosynth. Res. 81*, 165−180.
35. Kirmaier, C., Laible, P. D., Hanson, D. K., and Holten, D. (2004) B-side electron transfer to form $P^+H_B^-$ in reaction centers from the F(L181)Y/Y(M208)F mutant of *Rhodobacter capsulatus*, *J. Phys. Chem. B 108*, 11827−11832.
36. Wakeham, M. C., Breton, J., Nabedryk, E., and Jones, M. R. (2004) Formation of a semiquinone at the QB site by A- or B-branch electron transfer in the reaction center from *Rhodobacter sphaeroides*, *Biochemistry 43*, 4755−4763.
37. Breton, J., Wakeham, M. C., Fyfe, P. K., Jones, M. R., and Nabedryk, E. (2004) Characterization of the bonding interactions of Q_B upon photoreduction via A-branch or B-branch electron transfer in mutant reaction centers from *Rhodobacter sphaeroides*, *Biochim. Biophys. Acta 1656*, 127−138.
38. Paddock, M. L., Chang, C., Xu, Q., Abresch, E. C., Axelrod, H. L., Feher, G., and Okamura, M. Y. (2005) Quinone (Q_B) reduction by B-branch electron transfer in mutant bacterial reaction centers from *Rhodobacter sphaeroides*: Quantum efficiency and X-ray structure, *Biochemistry 44*, 6920−6928.
39. Frolov, D., Wakeham, M. C., Andrizhiyevskaya, E. G., Jones, M. R., and van Grondelle, R. (2005) Investigation of B-branch electron transfer by femtosecond time-resolved spectroscopy in a *Rhodobacter sphaeroides* reaction centre that lacks the Q_A ubiquinone, *Biochim. Biophys. Acta 1707*, 189−198.
40. Wakeham, M. C., and Jones, M. R. (2005) Rewiring photosynthesis: engineering wrong-way electron transfer in the purple bacterial reaction center, *Biochem. Soc. Trans. 133*, 851−857.
41. Wakeham, M. C., Frolov, D., Fyfe, P. K., van Grondelle, R., and Jones, M. R. (2003) Acquisition of photosynthetic capacity by a reaction centre that lacks the Q_A ubiquinone; possible insights into the evolution of reaction centres? *Biochim. Biophys. Acta 1607*, 53−63.
42. Volk, M., Aumeier, G., Langenbacher, T., Feick, R., Ogrodnik, A., and Michel-Beyerle, M. E. (1998) Energetics and mechanism of primary charge separation in bacterial photosynthesis. A comparative study on reaction centers of *Rhodobacter sphaeroides* and *Chloroflexus aurantiacus*, *J. Phys. Chem. B 102*, 735−751.
43. Parson, W. W., Clayton, R. K., and Cogdell, R. J. (1975) Excited states of photosynthetic reaction centers at low redox potentials, *Biochim. Biophys. Acta 387*, 265−278.
44. Chidsey, C. E. D., Kirmaier, C., Holten, D., and Boxer, S. G. (1984) Magnetic field dependence of radical-pair decay kinetics and molecular triplet quantum yield in quinone-depleted reaction centers, *Biochim. Biophys. Acta 766*, 424−437.
45. Woodbury, N. W., and Parson, W. W. (1984) Nanosecond fluorescence from isolated photosynthetic reaction centers of *Rhodopseudomonas sphaeroides*, *Biochim. Biophys. Acta 767*, 345−361.
46. Ogrodnik, A., Volk, M., Letterer, R., Feick, R., and Michel-Beyerle, M. E. (1988) Determination of the free energies in reaction centers of *Rb. sphaeroides*, *Biochim. Biophys. Acta 936*, 361−371.
47. Peloquin, J. M., Williams, J. C., Lin, X., Alden, R. G., Taguchi, A. K. W., Allen, J. P., and Woodbury, N. W. (1994) Time-dependent thermodynamics during early electron transfer in reaction centers from *Rhodobacter sphaeroides*, *Biochemistry 33*, 8089−8100.
48. Levine, L. M. A., and Holten, D. (1988) Axial-ligand control of the photophysical behavior of ruthenium(II) tetraphenylporphyrin and octaethylporphyrin − contrasting properties of metalloporphyrin (pi, pi-star) and (d-pi-star) excited-states, *J. Phys. Chem. 92*, 714−720.
49. Ogrodnik, A., Keupp, W., Volk, M., Aumeier, G., and Michel-Beyerle, M. E. (1994) Inhomogeneity of radical pair energies in photosynthetic reaction centers revealed by differences in recombination dynamics of P^+H^- when detected in delayed emission and in absorption, *J. Phys. Chem. 98*, 3432−3439.
50. Kirmaier, C., Laporte, L., Schenck, C. C., and Holten, D. (1995) The nature and dynamics of the charge-separated intermediate in reaction centers in which bacteriochlorophyll replaces the photoactive bacteriopheophytin. 2. The rates and yields of charge separation and recombination, *J. Phys. Chem. 99*, 8910−8917.
51. Kirmaier, C., Gaul, D., DeBey, R., Holten, D., and Schenck, C. C. (1991) Charge separation in a reaction center incorporating bacteriochlorophyll in place of photoactive bacteriopheophytin, *Science 251*, 922−927.
52. Heller, B. A., Holten, D., and Kirmaier, C. (1996) Effects of Asp residues near the L-side pigments in bacterial reaction centers, *Biochemistry 35*, 15418−15427.
53. Laporte, L., McDowell, L. M., Kirmaier, C., Schenck, C. C., and Holten, D. (1993) Insights into the factors controlling the rates of the deactivation processes that compete with charge separation in photosynthetic reaction centers, *Chem. Phys. 176*, 615−629.

54. Tang, C.-K., Williams, J. C., Taguchi, A. K. W., Allen, J. P., and Woodbury, N. W. (1999) $P^+H_A^-$ charge recombination rate constant in *Rhodobacter sphaeroides* reaction centers is independent of P/P^+ midpoint potential, *Biochemistry 38*, 8794−8799.
55. Kirmaier, C., Laporte, L., Schenck, C. C., and Holten, D. (1995) The nature and dynamics of the charge-separated intermediate in reaction centers in which bacteriochlorophyll replaces the photoactive bacteriopheophytin. 1. Spectral characterization of the transient state, *J. Phys. Chem. 99*, 8903−8909.
56. Heller, B. A., Holten, D., and Kirmaier, C. (1995) Characterization of bacterial reaction centers having mutations of aromatic residues in the binding site of the bacteriopheophytin intermediary electron carrier, *Biochemistry 34*, 5294−5302.
57. Connolly, J. S., Gorman, D. S., and Seely, G. R. (1973) Laser flash photolysis studies of chlorin and porphyrin systems. I. Energetics of the triplet state of bacteriochlorophyll, *Ann. N. Y. Acad. Sci. 206*, 649−669.
58. Holten, D., Gouterman, M., Parson, W. W., Windsor, M. W., and Rockley, M. G. (1976) Electron transfer from photoexcited singlet and triplet bacteriopheophytin, *Photochem. Photobiol. 23*, 415−423.
59. Chidsey, C. E. D., Takiff, L., Goldstein, R. A., and Boxer, S. G. (1985) Effect of magnetic fields on the triplet state lifetime in photosynthetic reaction centers: evidence of thermal repopulation of the initial radical Pair, *Proc. Natl. Acad. Sci. U.S.A. 82*, 6850−5854.
60. Sporlein, S., Zinth, W., Meyer, M., Scheer, H., and Wachtveitl, J. (2000) Primary electron transfer in modified bacterial reaction centers: optimization of the first events in photosynthesis, *Chem. Phys. Lett. 322*, 454−464.
61. Shkurapatov, A. Y., and Shuvalov, V. A. (1993) Electron transfer in pheophytin a-modified reaction centers from *Rhodobacter sphaeroides* R-26, *FEBS Lett. 322*, 168−172.
62. Schmidt, S., Arlt, T., Hamm, P., Huber, H., Nagele, T., Wachtveitl, J., Meyer, H., Scheer, H., and Zinth, W. (1994) Energetics of the primary electron-transfer reaction revealed by ultrafast spectroscopy on modified bacterial reaction centers, *Chem. Phys. Lett. 223*, 116−120.
63. Kennis, J. T. M., Shkuropatov, A. Y., van Stokkum, I. H. M., Gast, P., Hoff, A. J., Shuvalov, V. A., and Aartsma, T. J. (1997) Formation of a long-lived $P^+B_A^-$ state in plant pheophytin-exchanged reaction centers of *Rhodobacter sphaeroides* R26 at low temperature, *Biochemistry 36*, 16231−16238.
64. Huber, H., Meyer, M., Nagel, T., Hartl, I., Scheer, H., Zinth, W., and Wachtveitl, J. (1995) Primary photosynthesis in reaction centers containing four different types of electron acceptors at site H_A, *Chem. Phys. Lett. 197*, 297−305.

BI060277X